Rydberg states with anisotropic ion cores: Stark effect

D. E. Kelleher[*]

Joint Institute for Laboratory Astrophysics, University of Colorado and National Bureau of Standards,
Boulder, Colorado 80309-0440

E. B. Saloman

Center for Radiation Research, National Bureau of Standards, Gaithersburg, Maryland 20899

We have measured the Stark spectra of $5d_{3/2}8l$ autoionizing states in barium. Because of the anisotropic $5d$ ion core, the Stark manifolds at higher fields are considerably more complex than those for the analogous $6snl$ bound states. The electrostatic coupling of the Rydberg electron with the anisotropic core gives rise to relatively large fine-structure splittings. For nonpenetrating orbitals $(l_{Ry} > l_{core})$, jK coupling is a useful representation and the number of fine-structure components due to this interaction with the core increases the number of eigenstates $(2j_{core} + 1)$-fold. We present a theoretical model for the calculation of Stark spectra in jK coupling. Results for barium are in quantitative agreement with the experimental observations for both π and σ polarizations up to fields where there is extensive overlap between adjacent n manifolds. These fine-structure effects occur for any states with nonisotropic cores $(j_{core} > \frac{1}{2})$, i.e., the states of most atoms except for bound singly excited states of alkali-metal and alkaline-earth-metal atoms.

I. INTRODUCTION

In the past decade extensive measurements have been made of the Stark effect on bound Rydberg levels of alkali-metal and alkaline-earth-metal atoms.[1,2] For high nl states, which are hydrogenic, a so-called "Stark manifold" is observed in which the energies of the levels fan out approximately linearly as a function of field. Deviation from this hydrogenic behavior depends on the size of the quantum defect of the state, which decreases rapidly with l. Thus s- and p- state energies have a nonhydrogenic quadratic-field dependence until they anticross with a state in a linear manifold. Higher-l states tend to be quasihydrogenic. Also, for a given M symmetry, where M is the total magnetic quantum number, levels do not cross, and frequent avoided crossings are observed as the field is increased.

In the following discussion we refer to the orbital and total angular momentum of the ionic core as l_c and j_c, respectively, and the orbital angular momentum of the Rydberg electron outside the ionic core as l. In the cases mentioned in the above paragraph, $l_c = 0$, $j_c = \frac{1}{2}$. The fine structure in these cases, due to the spin-orbit interaction of the Rydberg electron, is generally quite small and has a small effect on the Stark manifolds.[2] In atoms with $j_c > \frac{1}{2}$, additional fine structure arises from the electrostatic interactions between the Rydberg electron and the ionic core, which are due to the nonspherical symmetry of the core (quadrupole and higher moment interactions, and tensor polarizability of the core).[3] This fine structure is generally substantially larger than the spin-orbit fine structure, and often comparable to or larger than the quantum defects for the higher-l Rydberg states. The analysis below builds on the work in Refs. 3—6.

This fine structure has two principal effects on the Stark manifold: (1) It breaks the quasidegeneracy of the higher l levels at low fields. The field dependence of the manifold does not become linear until a field is reached where the Stark shifts exceed the fine-structure splittings. (2) The most dramatic effect of the fine structure is that it gives rise to many more components in the Stark manifold. These come from the different possible couplings of the angular momenta associated with the electrostatic interaction between the Rydberg electron and the anisotropic core.

From a given lower level, most of the fine-structure levels are observable only at higher fields. Thus, as the field is increased, more and more components appear. Two or more components appear to grow or split off from a single component at lower field. The effect of this can be seen by comparing the computed barium-energy Stark spectra as seen in Fig. 1 [$n = 8$ (Rydberg electron); $j_c = \frac{1}{2}$ (isotropic core)] with Fig. 2 [$n = 8$ (Rydberg electron); $j_c = \frac{3}{2}$ (anisotropic core)]. The Stark manifolds for $j_c > \frac{1}{2}$ are sufficiently more complex than the $j_c = \frac{1}{2}$ case that we have chosen to examine an $n = 8$ manifold with $j_c = \frac{3}{2}$. The $n \sim 15$ manifold examined in the $l_c = 0$ cases[1] would be too complex for straightforward analysis. The fact that the levels we have studied are autoionizing is incidental; our focus in this paper is the effect of the core anisotropy on the atomic structure, as manifested in a Stark field. The theoretical model should apply equally well to bound levels with anisotropic cores.

II. THEORETICAL TREATMENT

The electrostatic interaction between the "core" electron and the Rydberg electron is greatly simplified in the
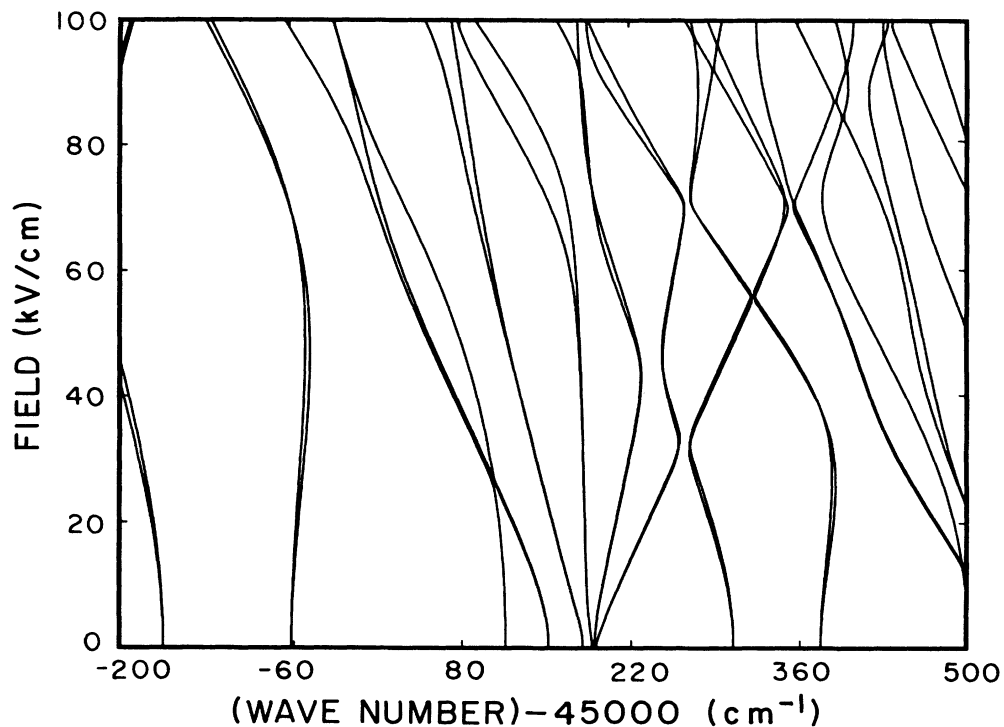
FIG. 1. Theoretical $M = 0$ Stark map in the region of the $6s_{1/2}8l$ autoionizing levels of Ba I. This spectrum, which lacks the fine structure due to an anisotropic core, should be contrasted with the much more complex spectrum in Fig. 2. For purposes of comparison, the energies are fictitiously scaled up to the values they would have if the $6s_{1/2}$ limit was equal to the $5d_{3/2}$ limit.
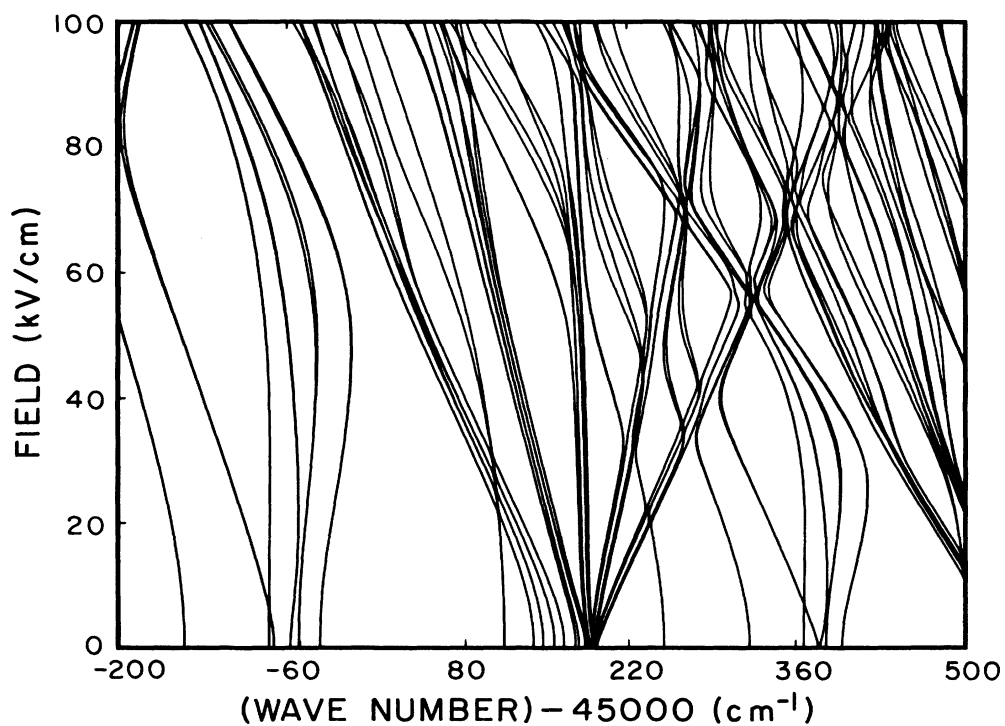

FIG. 2. Theoretical $M = 0$ Stark map in the region of the $5d_{3/2}8l$ autoionizing levels of Ba I. There are $2j_c + 1 = 4$ times as many components as in the $j_c = \frac{1}{2}$ spectrum of Fig. 1, due to the different angular-momentum couplings that arise between the Rydberg electron $(8l)$ and the $5d_{3/2}$ core electron.

nonpenetrating orbital approximation. The electrostatic "direct" interaction energy is given by

$$\sum_{k}^{\text{even}} f_k F^k ,$$ (1)

where, in the limit that the Rydberg electron does not significantly penetrate the core,

$$F^k = \langle r_c^k \rangle \langle r^{-(k+1)} \rangle .$$ (2a)

The angular part of the interaction is

$$f_k = \langle JM\beta \mid \mathbf{C}^{(k)}(\theta,\phi) \cdot \mathbf{C}^{(k)}(\theta_c,\phi_c) \mid J'M'\beta' \rangle .$$ (2b)

Corrections to F^k due to wave-function overlap (core penetration) are discussed in Appendix A. $\langle r_c^k \rangle$ is related to the kth multipole of the ionic core (e.g., quadrupole for $k = 2$). Hydrogenic values are commonly used for $\langle r^{-(k+1)} \rangle$. Terms in the sum over k in Eq. (1) are nonvanishing only for k even and $k \leq 2l_c$. The $k = 0$ term influences the average energy, and does not contribute to fine structure. For atoms with isotropic cores, only the $k = 0$ term exists. In the nonpenetrating orbital case $(l > l_c)$, the exchange interaction can generally be neglected.

In addition to the electrostatic interaction between the "unperturbed" one-electron orbitals given in Eq. (1), there also exists a polarization energy associated with the distortion of the orbitals due to the electrostatic interaction. The so-called scalar polarizability α affects the average energy of a multiplet; it is usually the dominant constituent of the quantum defect for nonpenetrating orbitals. The anisotropic polarizability γ_t, in contrast, affects only the fine structure of a multiplet, and not the average energy.

The angular part of both the quadrupole and anisotropic polarizability is given by the same second-rank tensor

$$\mathbf{C}^{(2)}(\alpha_{12}) = \mathbf{C}^{(2)}(\theta_1,\phi_1) \cdot \mathbf{C}^{(2)}(\theta_2,\phi_2) ,$$

where α_{12} is the angle between the two electron vectors r_1, r_2, and (θ_i, ϕ_i) are the spherical angles for each vector. As described in Appendixes A and B, and in Ref. 3, Eqs. (7) and (8), the lowest-order electrostatic fine-structure splittings about the mean energy are given in atomic units by

$$\Delta E = -f_2 \left[\langle r_c^2 \rangle \langle r^{-3} \rangle + \frac{\gamma_t}{3} \langle r^{-4} \rangle \right] + O(\langle r^{-5} \rangle) ,$$

                                                                                            (3)

where $\langle r_c^2 \rangle$ is the mean-square radius of the core, related to its quadrupole moment, and γ_t is the anisotropic polarizability of the core. The mean values $\langle r^{-3} \rangle$ and $\langle r^{-4} \rangle$ of the Rydberg electron can be approximated by the hydrogenic formulas[7]

$$\langle r^{-3} \rangle = \frac{Z^3}{n^3 (l+1)(l+\frac{1}{2})l} ,$$ (4a)

$$\langle r^{-4} \rangle = \frac{Z^4 (\frac{1}{2})[3n^2 - l(l+1)]}{n^5 (l+\frac{3}{2})(l+1)(l+\frac{1}{2})l(l-\frac{1}{2})} .$$ (4b)

The evaluation of the angular part f_k is best accomplished by choosing an angular-momentum coupling scheme well suited to the problem. The subspace β in Eq. (2b) should consist of quantities that are relatively good quantum numbers, so that off-diagonal terms are small. For a "non-penetrating" Rydberg orbital around a nonisotropic core, jK coupling is often the most judicious choice. Validity criteria for jK coupling are described below.

Treatment of the Stark effect for Rydberg levels with nonspherical cores is straightforward in the jK representation, first introduced by Racah.[8] j is the total angular momentum of the core, which we refer to as j_c. The K's are the result of different possible couplings between j_c and l:

$$\mid l - j_c \mid \leq K \leq \mid l + j_c \mid .$$

The number of K's is equal to $2j_c + 1$ (or $2l + 1$ if $l < j_c$). K is the vector sum of all the angular momenta except for the spin of the outside "Rydberg" electron. The total angular momentum is $J = K \pm \frac{1}{2}$. jK coupling is also referred to as "pair" coupling; when jK coupling is valid, the two values of J associated with a given K are very close in energy, forming a pair.

jK coupling is a useful approximation when the fine-structure splitting of the ionic core is large compared to both the direct and exchange energy of the Rydberg electron with the core, and the exchange energy is in turn small compared to the direct energy. Thus if the splittings among different fine-structure components of a given nl Rydberg state are small compared to the fine-structure splitting of the ion core, jK coupling is a good approximation. One must also exclude cases in which configuration interaction due to an interloper or a "crossing" with Rydberg series having a different core perturbs the energy of the level by an amount significant compared to the fine-structure splitting of the ion core. With the exception of the very lowest members of the series, Rydberg levels are usually well described by jK coupling. Since the Rydberg fine structure scales $\sim n^{-3}$ and even more strongly with l, one normally need not go far up the Rydberg scale before jK coupling is a good approximation.

jK coupling is useful in the present case of a nonpenetrating orbit around an anisotropic core because the fact that it is nonpenetrating means that the spin-orbit interaction of the Rydberg electron is usually small compared to the spin-orbit interaction of the core and to the noncentral electrostatic interaction between the Rydberg electron and the core. The latter is diagonal in jK coupling to the extent that spin-orbit coupling and exchange are negligible compared to the direct interaction, which is usually the case for nonpenetrating orbitals.

The angular part of the coupling is given by f_2, which in jK coupling is given by Racah:[8]

$$f_2 = \frac{6h^2 + 3h - 2j_c(j_c+1)l(l+1)}{4j_c(j_c+1)(2l-1)(2l+3)} ,$$ (5a)

where

$$h = \frac{1}{2}[K(K+1) - j_c(j_c+1) - l(l+1)] \equiv \mathbf{j}_c \cdot \mathbf{l} .$$ (5b)

Note that f_2 depends only on j_c of the core and not on l_c. However, it is important to note that Eqs. (2)—(5) apply only to two-electron coupling, i.e., a single Rydberg electron is interacting with one electron (or hole) in the open shell of the core. The above expression for f_2 is somewhat different from Eq. (11) of Ref. 3, which does not include the effect of the fine structure of the core. This effect is important for the atomic problem. A derivation of Racah's result for f_2 [Eq. (5)] is given in Appendix B.

The field coupling between two levels is equal to the field F times the expectation value of the electric dipole operator $z = P_0^{(1)}$. Using the Wigner-Eckart theorem,[9] it can be expressed (in atomic units) as

$$
\begin{aligned}
\langle H_F \rangle &= \langle \gamma M J \,|\, F P_0^{(1)} \,|\, \gamma M'J' \rangle \\
&= -F(-1)^{J-M}
\begin{bmatrix} J & 1 & J' \\ -M & 0 & M \end{bmatrix}
\langle \gamma J || \mathbf{P}^{(1)} || \gamma'J' \rangle \ .
\end{aligned}
\tag{6}
$$

The reduced dipole operator matrix element is given by[9]

$$
\begin{aligned}
\langle \alpha J || \mathbf{P}^{(1)} || \alpha'J' \rangle &= (-1)^{J'-j_c+1/2+l-l'+l_>} l_>^{1/2} \\
&\quad \times \langle nl \,|\, r \,|\, n'l' \rangle \\
&\quad \times [J,J'K,K']^{1/2}
\begin{vmatrix} \frac{1}{2} & J & K \\ 1 & K' & J' \end{vmatrix} \\
&\quad \times
\begin{Bmatrix} j_c & 1 & K \\ 1 & K' & l' \end{Bmatrix}
\end{aligned}
\tag{7}
$$

where $[J] \equiv 2J+1$, $[J,J'] = [J][J']$, etc., and $l_>$ is the larger of l,l'. Standard notation for the 3-j and 6-j symbols has been used. The selection rules are

$$\Delta K = 0, \pm 1 \quad (\text{no } K = 0 \rightarrow K' = 0) \ ,$$

$$l' = l \pm 1 \ ,$$

$$\Delta j_c = 0 \quad (\text{also } \Delta l_c, \Delta S_c = 0) \ ,$$

$$\Delta M = 0 \ .$$

Analytical expressions for the 3-j symbol are given in Appendix C.

Computation of the Stark spectrum is done in four steps: (1) Compute the zero-field energies by determining the mean energy from the quantum defect $\delta(l)$, and the electrostatic fine-structure splitting from Eq. (3). (2) Evaluate the angular matrix elements in Eqs. (6) and (7). (3) Evaluate the radial matrix element in Eq. (7) using the Coulomb approximation.[10] (4) Diagonalize the energy matrix.

The above steps are sufficient to yield the eigenenergies in the presence of a field. In order to obtain spectra that can be compared in detail with experiment, we must also compute: (5) the oscillator strengths from a given lower level and (6) the field-induced enhancement or suppression of the autoionizing widths for each level. Details of these calculations, especially (5) and (6), are discussed below.

The basis states include the $nlKJ$ states of the n manifold of interest, plus the nearest manifold below and the two above (because they are closer in energy), plus states

from higher n, low l, with sufficiently large quantum defect that they fall in this energy range (in zero field). Specifically, we include those states with $n^* = n - \delta_l$ such that $(n-1.5) < n^* < (n+2.2)$, where n is the principal quantum number of central interest. The total number of basis states is approximately $4n(4j_c+1)$. In our case of $n = 8$, $j_c = \frac{3}{2}$, we included 228 basis states.

The above procedure yields the eigenenergies in the presence of the field, and the expansion coefficients for the eigenstates ψ_j in terms of the zero-field basis states ϕ_i:

$$\psi_j(F) = \sum_i \alpha_{ij}(F)\phi_i \ . \tag{8}$$

The observable in the experiment is the photoion spectrum due to laser excitation from some lower state ψ_0. For the neutral atom considered here the autoionization decay rate of the excited levels is much larger than their radiative decay rate so that the ion-yield spectrum should be proportional to the photoabsorption spectrum. The electric dipole transition probability A_j for photoabsorption from ϕ_0 to the autoionizing level ψ_j is

$$A_j = \left| \sum_i \alpha_{ij} \langle \phi_0 || \mathbf{P}^{(1)} || \phi_i \rangle \right|^2 \ , \tag{9}$$

where $\langle \mathbf{P}^{(1)} \rangle$ is evaluated using Eq. (7). The radial matrix elements in Eq. (7) were evaluated using the Coulomb approximation. This is a poor approximation for a valence state like the $5d^2\,^1S_0$ lower level in our experiment. For such a state, indeed especially for states involving equivalent electrons, representing the effect of electron correlations by a quantum defect is a crude approximation at best. The result is that the relative intensities computed from Eq. (9) are only good to within a factor of about 2 or 3 at lower fields, and significantly worse at higher fields, where extensive mixing occurs. The field-dependent relative intensities can be particularly sensitive to errors in the radial matrix elements because of the interferences that occur in Eq. (9). This approximate treatment is still quite useful in comparing with experimental spectra, however, because it can still give a rough idea of which components become observable at a given field. To improve significantly on this would require, at the least, a careful MCHF characterization of the $^1S_0$ state, which, due partly to the equivalent electrons, has not yet been successfully accomplished.

Unfortunately, accurate estimates of both $\langle r_c^2 \rangle$ and γ_t in Eq. (3) cannot be obtained from spectroscopic data alone. This is because the functional dependence on n, for a given l, of $\langle r^{-3} \rangle$ and $\langle r^{-4} \rangle$ [see Eq. (4)] is nearly the same except for the lowest value of l, for which the Rydberg model begins to break down. (Due to the dependence of the quantum defects on l, it is generally not practical to extract values of $\langle r_c \rangle$ and γ_t using spectroscopic data from different l levels.) Also, higher-order terms in Eq. (3) are not likely to be negligible; octupole and diabatic anisotropic polarizability $[O(r^{-6})]$ terms may be significant. For a detailed analysis of the different contributions to the fine structure, one requires not only spectroscopic data but also accurate theoretical estimates or supplementary data, such as polarizability data. We determined the

"effective" value of $\langle r_c^2 \rangle_{\text{eff}}$ for the Ba$^+$ $5d_{3/2}$ core from published zero-field fine-structure splittings. We define $\langle r_c^2 \rangle_{\text{eff}}$ by

$$\Delta E = -f_k(j_c, l, k) \langle r^{-3} \rangle \langle r_c^2 \rangle_{\text{eff}} . \tag{10}$$

This is an approximation to Eq. (3), which already does not include the octupolar interactions (which also exist for d states). However, the semiempirical value of $\langle r_c^2 \rangle_{\text{eff}}$ affords the best single-parameter estimate of the electrostatic interactions giving rise to fine structure. The effective value of $\langle r_c^2 \rangle$, $8.4a_0^2$, was obtained by fitting Eq. (10) to the zero-field energies of the $5d_{5/2}ng$ states (of different K) published by Camus et al.,[11] for $n = 5$ to 8.

Quantum defects were used to model the "average energies" $E_{n,l}$. The average energies or "center of gravity" of each n,l multiplet was found by subtracting out the fine-structure splitting of the fine-structure components, using Eq. (10). The energies E_{nl} are then determined in the usual way by $E_{nl} = R_\infty (1 - 1/n_l^{*2})$, $n_l^* = n - \delta_l$. If the fine structure is not first "removed," different members of a n,l multiplet will yield widely varying values of the single-channel quantum defect. The energies were taken from Refs. 11 and 12. The quantum defects for the $5d_{3/2}nl$ states for $l = 0, 1, 2, 3$, and 4 were in this way estimated to be 4.17, 3.72, 2.53, 0.0913, and 0.0268, respectively. The quantum defect for the $5d^2\,^1S_0$ state was 2.7160.

The focus of this paper is the effect of the anisotropic core on the Rydberg Stark manifold, and for this purpose the fact that the levels are autoionizing is secondary. Nevertheless, we have taken some measures to model the autoionizing rates (widths), and the effect of the field upon them. We estimated the zero-field widths by measuring the width of the $5d_{3/2}8f$ ($J = 1$) level ($\Gamma = 1.7$ cm^{-1}) and the scaling of the zero-field widths of the other $5d_{3/2}nl$ levels were estimated from data in Refs. 11 and 12. The field effect could be treated as in Ref. 13, the prediagonalization being accomplished in step 4 referred to above. However, the observed profiles are relatively symmetric, so that for our purposes direct transitions to the continuum may be ignored, and the width in the presence of a field should be adequately approximated by

$$\Gamma_j(F) = 2\pi \left| \sum_i \alpha_{ij}(F) V_i(F = 0) \right|^2 . \tag{11}$$

Here we have simply applied Eq. (8) together with the relation $\Gamma_j(F) = 2\pi |V_j(F)|^2$, where $V_j = \langle \phi_j(F) | r_{12}^{-1} | \psi_E \rangle$ is the configuration-interaction matrix element of the field-dressed state with the continuum ψ_E. We can infer the magnitude of the V_i's from the Γ_i's, but not their phase. We chose the phases of all the V_i's to be equal in generating the theoretical spectra shown in the results below. Different choices of phases resulted in observable but small differences in line shapes in the spectra; the overall qualitative features of the spectrum remain much the same, except in isolated regions at some fields where spurious interferences can occur. The values of the V_i's have, of course, no influence on the eigenenergies.

To summarize the principal approximations of our

model for the Rydberg Stark spectra for atoms having an anisotropic core: (i) We use the Coulomb approximation to evaluate the dipole matrix elements (this is expected to be quite accurate for the field coupling between Rydberg levels, and quite inaccurate for the photoexcitation rates between the $5d^2\,^1S_0$ state and the Rydberg levels). (ii) We estimate the electrostatic interactions arising from the anisotropy of the ionic core (quadrupole and octupole in the case of a d core, and anisotropic core polarizability) as an effective quadrupole term. (iii) For autoionizing levels, we assume that all the (zero-field) electrostatic couplings V_{E_i} between the Rydberg levels and the continua have the same phase.

In spite of these approximations, we see in Sec. III that the fine-structure spectrum that arises from the core anisotropy, which becomes manifest in an electric field, is reasonably well described by our model. While the theoretical approach involves parameters such as multipole moments of the core and quantum defects, these are not "adjustable" parameters. They are estimated by zero-field spectroscopic data, as described above.

III. EXPERIMENT

The experimental arrangement is the same as in Ref. 13, except that different final states were chosen. A radiatively heated oven at 610 °C generated a barium vapor that was collimated to form an atomic beam of $\sim 10^8$ atoms/cm^3 in a background gas pressure of 2×10^{-7} Torr. The temperature of the oven was servo-stabilized to ± 0.1 °C. Using a spherical mirror, three lasers were overlapped in the region of the beam. The barium atoms were stepwise excited via $6s^2\,^1S_0 \to 6s6p\,^3P_1^\circ \to 5d^2\,^1S_0 \to 5d_{3/2}8l$ (see Fig. 3). The latter states lie in the continuum above the $6s_{1/2}$ Ba$^+$ threshold and the $l = 3$ ($J = 1$) autoionizing width was measured to be 1.7 cm^{-1}. The three Nd:YAG pumped dye lasers (where YAG represents yttrium aluminum garnet) were of the near-grazing-incidence type with prism beam expanders and a bandwidth of 0.15 cm^{-1}. In the above excitation scheme, photons from the first two lasers lack sufficient energy to one-photon ionize the intermediate $5d^2\,^1S_0$ state, so that no background ionization was observed. The energy of the final laser was kept low to prevent spurious broadening due to depletion of the $5d^2\,^1S_0$ level. The final of the three lasers was scanned over the spectral region of interest at each field. Ions were collected through a mesh-covered hole in the center of one of the two 4-in.-diam. discs, between which the atomic beam passed; the dc field was applied between the discs. The ions impinged on the first dynode of a linear-array EMI electron multiplier D-233B. The amplified current pulse was fed into one channel of a gated digital-to-analog converter, a signal proportional to the amplitude of the final laser was fed into a second channel, and the average of these channels over 20 laser shots was stored by the computer at each computer-scanned wavelength. The photo-ion signal was normalized against the final laser intensity at each wavelength. The sine bar of the scanning dye laser was calibrated using a wavemeter and was checked against Ar I lines using opto-galvanic detection in a hollow cathode.
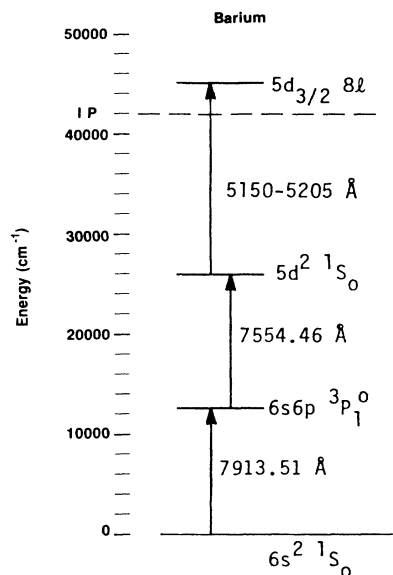
FIG. 3. Laser excitation scheme. The final laser was scanned over the spectral region of interest.

IV. RESULTS AND DISCUSSION

The experimental spectra obtained at different fields shown in Fig. 4 correspond to π polarization (linearly polarized laser field parallel to the dc field). Because the intermediate state is $J = 0$, $M = 0$, the π polarization corresponds to an $M = 0$ final state.

A Stark map showing the energies of all the eigenstates

in this spectral region as a function of field is shown in Fig. 5. In the energy spectrum shown, only one resonance is observable from the $5d^2\,{}^1S_0$ intermediate state at zero field. This is the $5d_{3/2}8f$ $(J=1)$ which in jK coupling has the "labels" $j_c = \frac{3}{2}$, $l = 3$, $K = \frac{3}{2}$, and $J = 1$. Usually a given $j_c lJ$ level will correspond to two K states, $K = J \pm \frac{1}{2}$, but only those K's exist that also satisfy $|l - j_c| \leq K \leq |l + j_c|$, which in the present case means that the lowest K value is $\frac{3}{2}$.

The predominant feature of the $5d_{3/2}8l$ Stark manifold is the gradual proliferation of observed levels as the field is increased. In absorption from the $5d^2\,{}^1S_0$ level, only the $5d_{3/2}8f$ $(J=1, K=\frac{3}{2})$ level is observed at zero field. At low fields (≤ 20 kV/cm), the levels that dipole couple to this level appear. As the field is further increased, each of these levels appears to split up into more components, until there are approximately $2n(2j_c + 1)$ components observed for each Stark manifold, not all of which are resolved. This "procreative" manifold originates from the coupling of the angular momentum of the Rydberg electron with that of the ion core. This coupling is due to the core anisotropy and arises via the r_{12}^{-1} interaction and anisotropic polarizability.

The widths of most of the components are observed to increase at the larger fields. This is especially pronounced at fields above which the adjacent n manifolds begin to overlap, i.e., for $F(\text{a.u.}) \geq (3n^5)^{-1} = 50$ kV/cm for $n = 8$. At such fields the narrow high-l states ($l \geq l_c$) mix (via anticrossings) extensively with the broader low-l states, leading to the broadening of the high-l states.[14]

Results from the theoretical model described above are shown for π polarization in Fig. 6. The qualitative
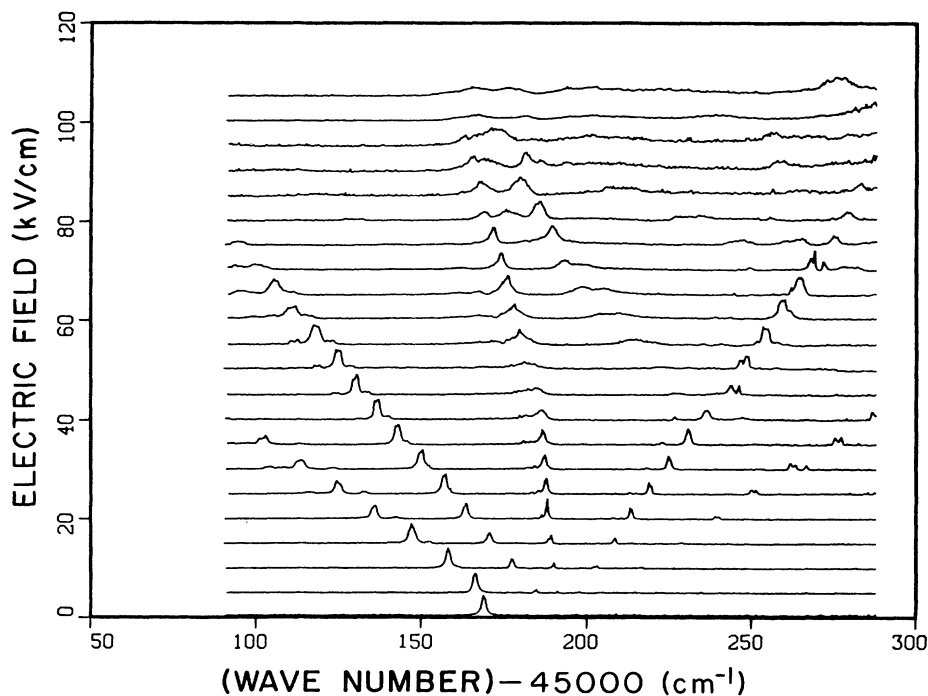

FIG. 4. Experimental photo-ion spectra from the $5d^5\,{}^1S_0$ state of Ba I at different electric fields, with π polarization (laser field parallel to applied dc field), in the region of the $5d_{3/2}8l$ autoionizing levels.
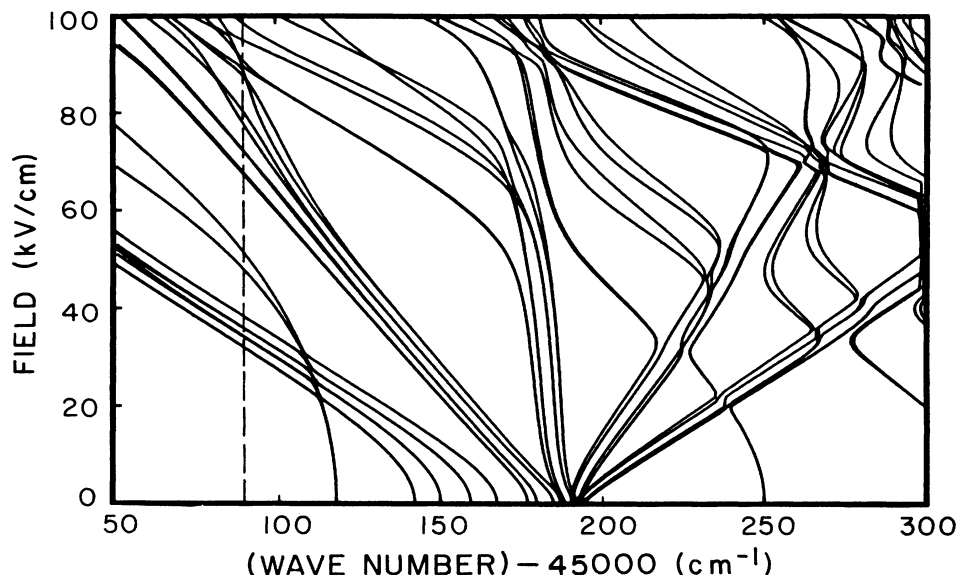
FIG. 5. $M = 0$ theoretical Stark map in the region of the $5d_{3/2}8l$ autoionizing levels of Ba I. This figure is a "detail" of Fig. 2, drawn on the scale of the experimental data. As seen in Fig. 4, most of these levels are only observed at higher fields. The $M = 1$ energy spectrum is almost identical.

features of the experimentally observed procreative Stark manifolds are reproduced in the theoretical spectra. In most cases the computed energies at fields $\lesssim 60$ kV/cm are off by small but observable amounts, which we attribute to the fact that we have not included the octupole term in Eq. (1), and to the fact that we have not explicitly included anisotropic polarizability effects.

The spectral dependence on M is subtle but well defined. In Fig. 7 (experimental) and Fig. 8 (theoretical) the $M = 1$ spectra obtained with σ polarization are presented.

In Fig. 9 (experimental) and Fig. 10 (theoretical) the π and σ spectra are superposed for a smaller region of the spectrum. It is clear that the dominant effect of π versus σ polarization is to enhance different subcomponents of a given fine-structure component.

Considering that only the lowest-order term in Eq. (1) has been used in estimating the fine-structure splitting, the quantitative agreement with the experimental spectra is quite satisfactory, at least for fields below ~ 50 kV/cm, beyond which there is extensive overlap between adjacent
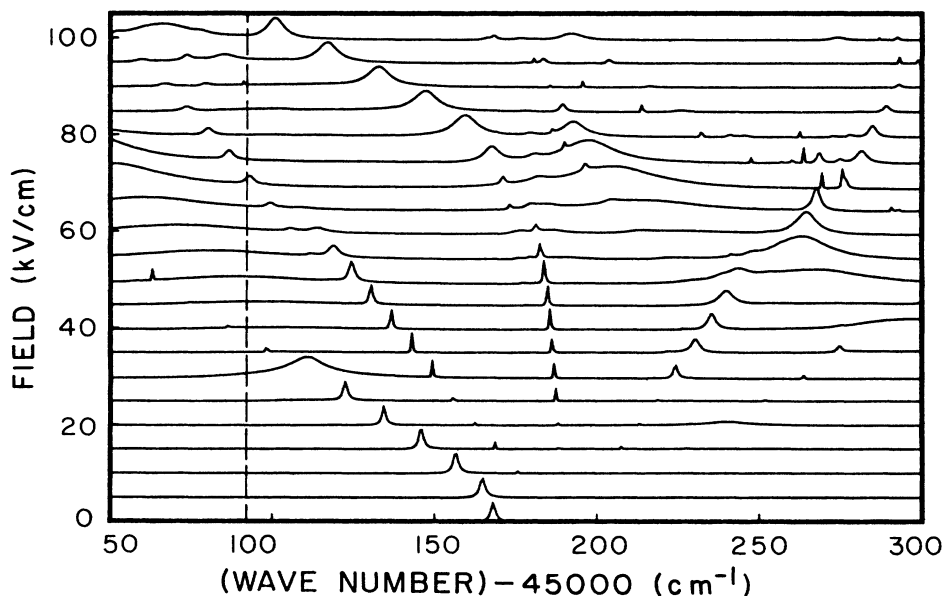

FIG. 6. Theoretical photo-ion spectra from the $5d^2\,^1S_0$ state of Ba I at different electric fields, with π polarization, in the region of the $5d_{3/2}8l$ autoionizing levels. The dashed line indicates the range of experimental observation.
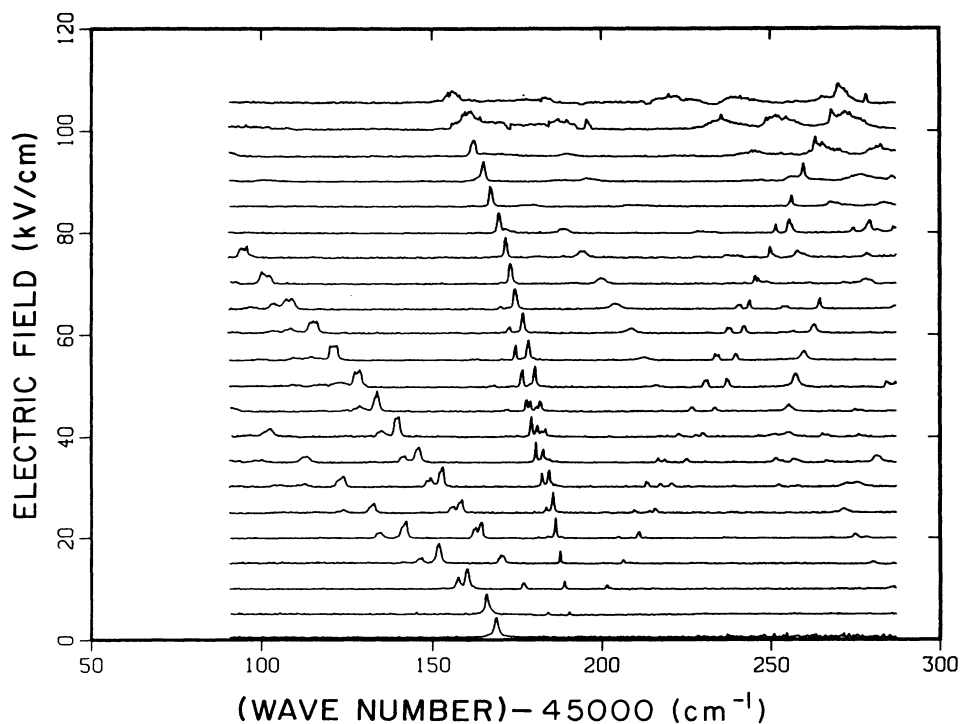
FIG. 7. Experimental photo-ion spectra from the $5d^2 {}^1S_0$ state of Ba I at different electric fields, with σ polarization (laser field perpendicular to applied dc field).

n manifolds. This includes the effect of the laser polarization with respect to the external dc field.

In conclusion, we note that the electrostatic coupling of a Rydberg electron with a nonisotropic ion core gives rise to a large number of fine-structure levels. As an applied electric field is increased, an increasing number of these levels become observable via dipole transitions from a given lower level, giving rise to a procreative Stark manifold. This problem can be efficiently treated in jK coupling. We emphasize that this fine structure, and the associated Stark effects, occurs not only for autoionizing levels, but for any states with nonisotropic cores ($j_c > \frac{1}{2}$), i.e., practically all levels of most atoms except for bound singly excited states of alkali-metal and alkaline-earth metal atoms. We note in closing that there is a clear need for the development of a useful method for computing tensor polarizabilities, with inclusion of nonadiabatic effects.
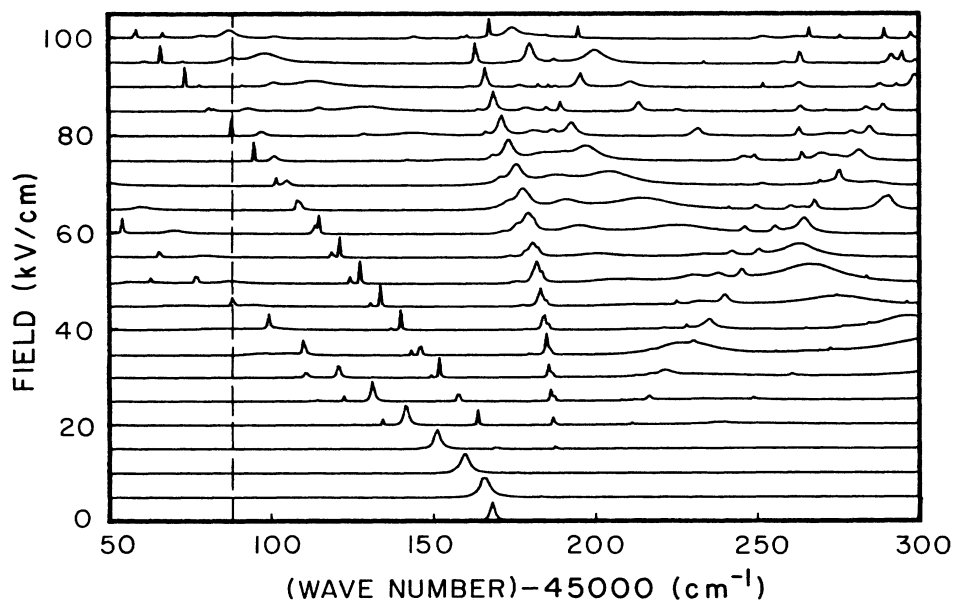

FIG. 8. Theoretical photo-ion spectra from the $5d^2 {}^1S_0$ state of Ba I at different electric fields, with σ polarization.

ACKNOWLEDGMENTS

APPENDIX A: MULTIPOLE APPROXIMATION TO THE SLATER INTEGRALS FOR NONPENETRATING ORBITALS

The electrostatic energy matrix, which gives the radial part of the kth order of the $1/r_{12}$ interaction, is

$$E^{1,2}_{1',2'} = \int_0^\infty \int_0^\infty \left\langle 1,2 \left| \frac{r^k_<}{r^{k+1}_>} \right| 1',2' \right\rangle d^3r_1 d^3r_2 . \qquad \text{(A1)}$$

Assuming in the usual way that the wave functions $|1,2\rangle$ are product wave functions $|1\rangle|2\rangle$, whose antisymmetry properties are contained in the exchange Slater integrals G^k, we can write the diagonal part of the direct interaction as

$$\sum_k f_k F^k , \qquad \text{(A2)}$$

where the direct Slater integral is

$$F^k = \int_0^\infty \langle 1 | r^k_1 | 1\rangle d'r_1 \int_{r_1}^\infty \langle r_2 | r^{-(k+1)}_2 | r_2\rangle d'r_2$$
$$+ \int_0^\infty \langle 2 | r^k_2 | 2\rangle d'r_2 \int_{r_2}^\infty \langle 1 | r^{-(k+1)}_1 | 1\rangle d'r_1 , \qquad \text{(A3)}$$

where $d'r \equiv r^2 dr$. Thus

$$F^k = \langle r^k_1\rangle\langle r^{-(k+1)}_2\rangle + \Delta^k , \qquad \text{(A4)}$$

where the brackets in (A4) indicate the usual expectation values, and the correction term Δ is given by

$$\Delta^k = \int_0^\infty \langle 2 | r^k_2 | 2\rangle d'r_2 \int_{r_2}^\infty \langle 1 | r^{-(k+1)}_1 | 1\rangle d'r_1$$
$$- \int_0^\infty \langle 1 | r^k_1 | 1\rangle d'r_1 \int_0^{r_1} \langle 2 | r^{-(k+1)}_2 | 2\rangle d'r_2 . \qquad \text{(A5)}$$

Applying the Dirichlet integral equality, we can also express Δ^k as

$$\Delta^k = \int_0^\infty \langle 2 | r^k_2 - r^{-(k+1)}_2 | 2\rangle d'r_2$$
$$\times \int_{r_2}^\infty \langle 1 | r^{-(k+1)}_1 - r^k_1 | 1\rangle d'r_1 . \qquad \text{(A6)}$$

The correction Δ^k will be small compared to F^k when the outer electron (labeled here as 2) does not significantly penetrate the orbital of the inner electron (labeled here as 1). This condition is usually satisfied if the orbital angular momentum of the "outer" electron exceeds that of the "inner" electron. Δ^k can be estimated using quantum-defect-theory approximations of the wave functions.

In the nonpenetrating orbital approximation, the direct Slater integral is thus approximated by

$$F^k \cong \langle r^k_<\rangle\langle r^{-(k+1)}_>\rangle , \qquad \text{(A7)}$$

where the subscripts $<$ and $>$ refer to the core and Rydberg electron, respectively. Hydrogenic forms of $\langle r^{-(k+1)}_>\rangle$ are frequently used. The kth moment of the ionic core, $\langle r^k_<\rangle$, can be estimated, for example, by computation or by fine-structure measurements. This relationship of F^k to the kth moment of the core has given rise to the multipolar description of the F^k's; for example, F^2 is often referred to as the quadrupolar interaction. Equation (A7) is just what one obtains from Eq. (A1) in the nonpenetrating orbital limit, where $r_2 > r_1$ for all r_2.

APPENDIX B: EVALUATION OF f_k IN jK COUPLING

The energy matrix elements of the two-electron interaction $1/r_{12}$, in the antisymmetrized product form of the wave function, give rise to the well-known direct and exchange integrals. The diagonal parts of the direct integrals have the form

$$\Delta E^{\text{dir}}_{\text{diag}} = \sum_k f_k F^k . \qquad \text{(B1)}$$

The multipolar approximation to the radial Slater integrals are discussed in Appendix A. The angular part of the diagonal direct interaction is contained in f_k:

$$f_k = \langle \alpha_1\alpha_2JM | \mathbf{C}^{(k)}(1)\cdot\mathbf{C}^{(k)}(2) | \alpha_1\alpha_2JM \rangle , \qquad \text{(B2)}$$

where $\mathbf{C}^{(k)}(1)$ and $\mathbf{C}^{(k)}(2)$ are kth order Racah tensors that operate only on the subspace of $|\alpha_1\rangle$ and $|\alpha_2\rangle$, respectively.

The f^k depend on the two-electron coupling scheme. In jK coupling, $\mathbf{K} = \mathbf{j}+\mathbf{l}$ is the product of coupling j, the total angular momentum of the core electron, and l, the orbital angular momentum of the outermost Rydberg electron. (K is then coupled to the spin, $\frac{1}{2}$, of the outer electron for J, the total angular momentum of the two-electron system.) For clarity, in the following we label quantum numbers of the core with the subscript c; unsubscripted quantities refer to the outer electron. Applying (C6) we can write
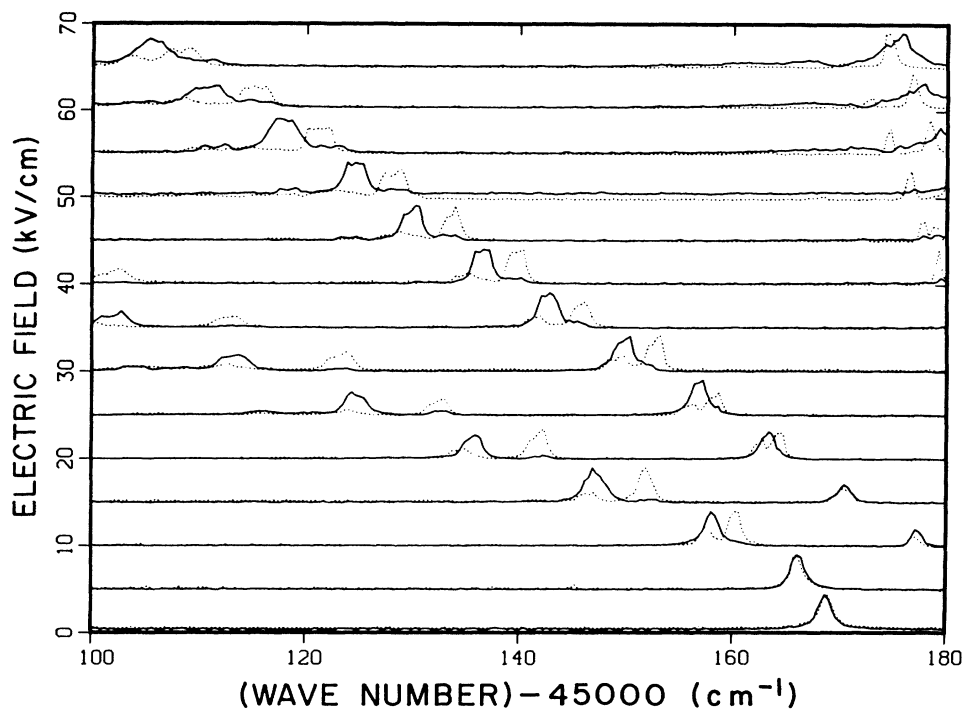
FIG. 9. Portion of experimental photo-ion spectra, with π (solid line) and σ (dotted line) polarization superposed.

$$\langle (l_c, \tfrac{1}{2})j_c, l[K]JM \mid \mathbf{C}^{(k)}(1) \cdot \mathbf{C}^{(k)}(2) \mid (l'_c, \tfrac{1}{2})j'_c, l'[K']J'M' \rangle$$

$$= \delta_{K,K'}(-1)^{j'_c + l + K} \begin{Bmatrix} K & l & j_c \\ k & j'_c & l' \end{Bmatrix} \langle (l_c, \tfrac{1}{2}), j_c \mid\mid \mathbf{C}^{(k)} \mid\mid (l'_c, \tfrac{1}{2}), j'_c \rangle \langle l \mid\mid \mathbf{C}^{(k)} \mid\mid l' \rangle \, . \quad \text{(B3)}$$

The Racah tensor $\mathbf{C}^{(k)}$ does not act on the spin ($\tfrac{1}{2}$), so that we may apply (C7) to get

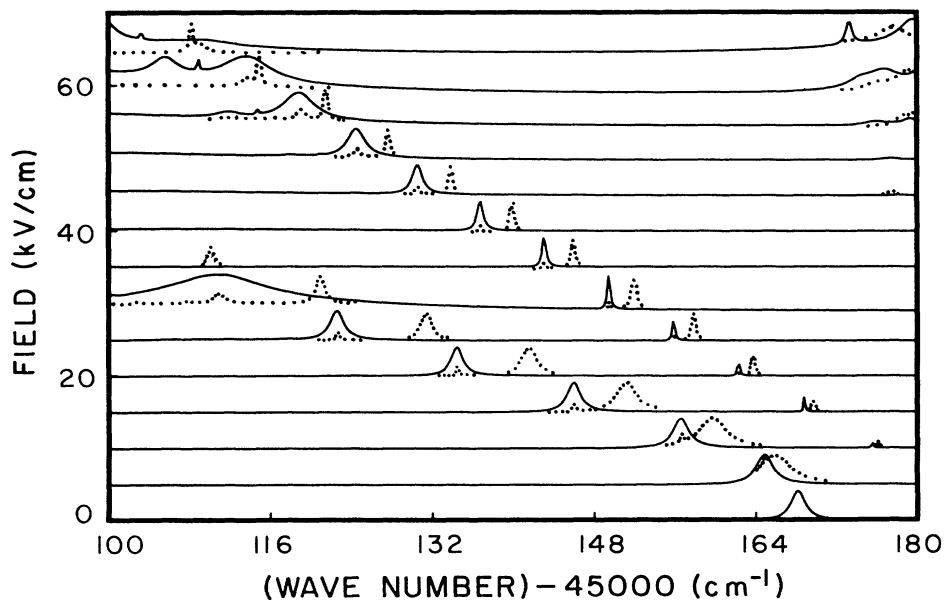FIG. 10. Portion of theoretical spectra with π (solid line) and σ (dotted line) polarization superposed.

$$\langle (l_c,\tfrac{1}{2})j_c,l[K]JM \mid \mathbf{C}^{(k)}(1)\cdot\mathbf{C}^{(k)}(2) \mid (l'_c,\tfrac{1}{2})j'_c,l'[K']J',M' \rangle$$

$$=\delta_{K,K'}[j_c,j'_c]^{1/2}(-1)^{K+l_c+l-1/2}\begin{Bmatrix} K & l & j_c \\ k & j'_c & l' \end{Bmatrix}\begin{Bmatrix} \tfrac{1}{2} & l_c & j_c \\ k & j'_c & l'_c \end{Bmatrix}\langle l_c||\mathbf{C}^{(k)}||l'_c\rangle\langle l||\mathbf{C}^{(k)}||l'\rangle \ , \tag{B4}$$

consistent with Eq. (7.19) of Ref. 15. Taking the diagonal elements and applying (C3), (C4), and (C5), we see that for the particular case $k=2$ this simplifies to

$$f_2=\frac{6h^2+3h-2j_c(j_c+1)l(l+1)}{4j_c(j_c+1)(2l-1)(2l+3)} \ , \tag{B5}$$

where $h=\tfrac{1}{2}[K(K+1)-j(j+1)-l(l+1)]$, a result first given by Racah.[8]

APPENDIX C: SOME REQUIRED RACAH ALGEBRA

Expressions from Edmonds[16] for the 3-j and 6-j symbols referred to in the text can be expressed in the following condensed form:

$$\begin{pmatrix} J & 1 & J \\ -M & 0 & M \end{pmatrix}=(-1)^{J-M}\frac{M}{[J(J+1)(2J+1)]^{1/2}} \ , \tag{C1}$$

$$\begin{pmatrix} J & 1 & J' \\ -M & 0 & M \end{pmatrix}=(-1)^{J_> -M}\left[\frac{J_>^2-M^2}{J_>(4J_>^2-1)}\right]^{1/2}, \quad J'=J\pm1 \ , \tag{C2}$$

$$\begin{Bmatrix} a & b & c \\ 2 & c & b \end{Bmatrix}=(-1)^{a+b+c}\frac{6h^2+3h-2b(b+1)c(c+1)}{[(2b-1)b(b+1)(2b+1)(2b+3)(2c-1)c(c+1)(2c+1)(2c+3)]^{1/2}} \ , \tag{C3}$$

where $h=\tfrac{1}{2}[a(a+1)-b(b+1)-c(c+1)]$. It can also be shown that

$$\begin{Bmatrix} \tfrac{1}{2} & b & c \\ 2 & c & b \end{Bmatrix}=(-1)^{b+c+1/2}\frac{1}{4}\left[\frac{(2b-1)(2b+3)(2c-1)(2c+3)}{b(b+1)(2b+1)c(c+1)(2c+1)}\right]^{1/2}. \tag{C4}$$

Also,

$$\langle l||\mathbf{C}^{(2)}||l\rangle=-\left[\frac{l(l+1)(2l+1)}{(2l-1)(2l+3)}\right]^{1/2}. \tag{C5}$$

Two well-known relations, used to derive expressions in Appendix B, are

$$\langle abJM \mid \mathbf{A}^{(k)}\cdot\mathbf{B}^{(k)} \mid a'b'J'M' \rangle=\delta_{\substack{JJ' \\ MM'}}(-1)^{a'+b+J}\begin{Bmatrix} J & b & a \\ k & a' & b' \end{Bmatrix}\langle a||\mathbf{A}^{(k)}||a\rangle\langle b||\mathbf{B}^{(k)}||a\rangle \ , \tag{C6}$$

where $\mathbf{A}^{(k)}$ operates only on the subspace a, and $\mathbf{B}^{(k)}$ only on the subspace b. The double bars indicate *reduced* matrix elements

$$\langle abJ||\mathbf{A}^{(k)}||abJ\rangle=\delta_{bb'}[J,J']^{1/2}(-1)^{a+b+J'+k}\begin{Bmatrix} b & a & J \\ k & J' & a' \end{Bmatrix}\langle a||\mathbf{A}^{(k)}||a'\rangle \ , \tag{C7}$$

where again $\mathbf{A}^{(k)}$ operates only on the subspace a.

*Permanent address: Center for Radiation Research, National Bureau of Standards, Gaithersburg, MD 20899.

[1]M. G. Littman, M. L. Zimmerman, T. W. Ducas, R. R. Freeman, and D. Kleppner, Phys. Rev. Lett. **36**, 788 (1976); M. L. Zimmerman *et al.*, J. Phys. B **11**, L11 (1978); D. Kleppner *et al.*, Sci. Am. **244**, 130 (1981).

[2]M. L. Zimmerman *et al.*, Phys. Rev. A **20**, 2251 (1979).

[3]E. E. Eyler and F. M. Pipkin, Phys. Rev. A **27**, 2462 (1983).

[4]R. D. Knight and L. Wang, Phys. Rev. A **32**, 896 (1985).

[5]S. M. Jaffe, R. Kachru, H. B. van Linden van den Heuvel, and

T. F. Gallagher, Phys. Rev. A **32**, 1480 (1985).

[6]E. S. Chang and H. Sakai, J. Phys. B **15**, L649 (1981).

[7]H. A. Bethe and E. E. Salpeter, *Quantum Mechanics of One- and Two-Electron Atoms* (Plenum, New York, 1977).

[8]G. Racah, Phys. Rev. **61**, 537 (1942).

[9]R. D. Cowan, *The Theory of Atomic Structure and Spectra* (University of California Press, Berkeley, California, 1981).

[10]The Coulomb approximation for radial dipole matrix elements was taken from the "Zimmerman code," details of which are discussed in Ref. 2.

[11]P. Camus, M. Dieulin, A. El Himdy, and M. Aymar, Phys. Scr. **27**, 125 (1983).

[12]R. D. Hudson and V. L. Carter, Phys. Rev. A **2**, 643 (1970).

[13]E. B. Saloman, J. W. Cooper, and D. E. Kelleher, Phys. Rev. Lett. **55**, 193 (1985).

[14]V. I. Mishin, G. G. Lombardi, J. W. Cooper, and D. E.

Kelleher, Phys. Rev. A **35**, 1664 (1986).

[15]B. W. Shore and D. H. Menzel, *Principles of Atomic Spectra* (Wiley, New York, 1968).

[16]A. R. Edmonds, *Angular Momentum in Quantum Mechanics*, 2nd ed. (Princeton University Press, Princeton, New Jersey, 1960).